

# MHD TURBULENCE AND COSMIC RAY REACCELERATION IN GALAXY CLUSTERS

ANDREY BERESNYAK

Los Alamos National Laboratory, Los Alamos, NM, 87545 and  
Ruhr-Universität Bochum, 44780 Bochum, Germany

HAO XU, HUI LI

Los Alamos National Laboratory, Los Alamos, NM, 87545

REINHARD SCHLICKEISER

Ruhr-Universität Bochum, 44780 Bochum, Germany

*Draft version August 9, 2021*

## ABSTRACT

Cosmological MHD simulations of galaxy cluster formation show a significant amplification of seed magnetic fields. We developed a novel method to decompose cluster magnetized turbulence into modes and showed that the fraction of the fast mode is fairly large, around 1/4 in terms of energy. This is larger than that was estimated before, which implies that cluster turbulence interacts with cosmic rays rather efficiently. We propose a framework to deal with electron and proton reacceleration in galaxy clusters that includes feedback on turbulence. In particular, we establish a new upper limit on proton and electron fluxes based on turbulence intensity. These findings, along with detailed modeling of reacceleration, will help to reconcile the observed giant radio haloes and the unobserved diffuse  $\gamma$ -ray emission from these clusters.

## 1. INTRODUCTION

Galaxy clusters are the largest virialized objects in the Universe. An important component of galaxy clusters is the intracluster medium (ICM), a hot gas between galaxies which is fully ionized and contains magnetic fields and cosmic rays (CRs). A number of observational techniques are used to detect various components of the ICM. Sunyaev-Zeldovich effect (e.g. Motl et al. 2005) and soft X-ray observations (e.g. see a review by McNamara & Nulsen 2007) are used to estimate hot gas temperature and density, radio observations of Faraday rotation in the ICM measure magnetic fields (e.g. Eilek & Owen 2002; Bonafede et al. 2010; Govoni et al. 2006, 2010). Radio observations of Mpc scale diffuse radio emissions, so called radio halos, indicate the presence of cluster-wide relativistic electrons in the ICM (e.g. Schlickeiser et al. 1987; Carilli & Taylor 2002; Ferrari et al. 2008; Giovannini et al. 2009; Feretti et al. 2012; van Weeren et al. 2012).

The diffuse gamma-ray emission from the ICM, which should come from interactions of the proton component of CRs and the gas, however, is not observed yet (Ackermann et al. 2010). As the lower limits to diffuse  $\gamma$ -ray emission are becoming better, it is harder to explain both diffuse radio haloes and the lack of diffuse  $\gamma$ -ray emission within a simple paradigm of the radio emission produced by secondary electrons (Reimer et al. 2004; Donnert et al. 2011; Brunetti & Lazarian 2011b). Since the lifetimes of synchrotron electrons are much shorter than their mixing time in the cluster, the in-situ reacceleration mechanism is very desirable. One of such mechanisms being considered is a turbulent second-order acceleration (see, e.g. Brunetti & Lazarian 2011a). Radio relics seen in some clusters (see, e.g., van Weeren et al. 2010) are thought to be associated

with large-scale shocks. The explanation of radio haloes as shocks in projection, however, can be excluded based on geometric arguments (Brunetti et al. 2008), or numerical simulations (Hoeft et al. 2008; Skillman et al. 2011; Vazza et al. 2011). The second-order acceleration by turbulence, therefore, should be considered as a viable candidate. The acceleration rate, which is proportional to  $(v_A/c)^2$  in the second order mechanism, was considered marginal in spiral galaxies, where  $v_A \sim 10 - 20$  km/s and the escape times from the relatively thin disk are short. In galaxy clusters, however, the Alfvénic speeds are higher  $v_A \sim 100$  km/s and the diffusion timescales are much longer due to their enormous size.

The early theoretical model seeking to explain the spectrum of the diffuse radio halo of the Coma cluster by Schlickeiser et al. (1987) used the combination of first and second order Fermi acceleration and radiative synchrotron and inverse Compton losses to produce a volume-integrated frequency spectrum which could be approximated as  $I(\nu) \propto \nu^{(3-\Gamma)/2} \exp(-\sqrt{\nu/\nu_c})$ , with parameters  $\Gamma$  and  $\nu_c$ , defined in the aforementioned paper, depending on the details of the embedded shocks and the functional dependence of the diffusion coefficients in energy. The above spectrum fits observations better than the single- and double-power laws characteristic of the primary (Jaffe 1977; Rephaeli 1977) and secondary electron models (Jaffe 1977; Dennison 1980). The cutoff frequency depends on a number of parameters such as magnetic field, density, spatial diffusion coefficient and the level of the background radiation field. Although a small fraction of galaxy clusters have radio halos (Feretti et al. 2012), this fraction is higher for bright clusters (Giovannini et al. 1999; Cassano et al. 2007).

As a technique complementary to observations, full cosmological simulations of cluster formation and evolu-

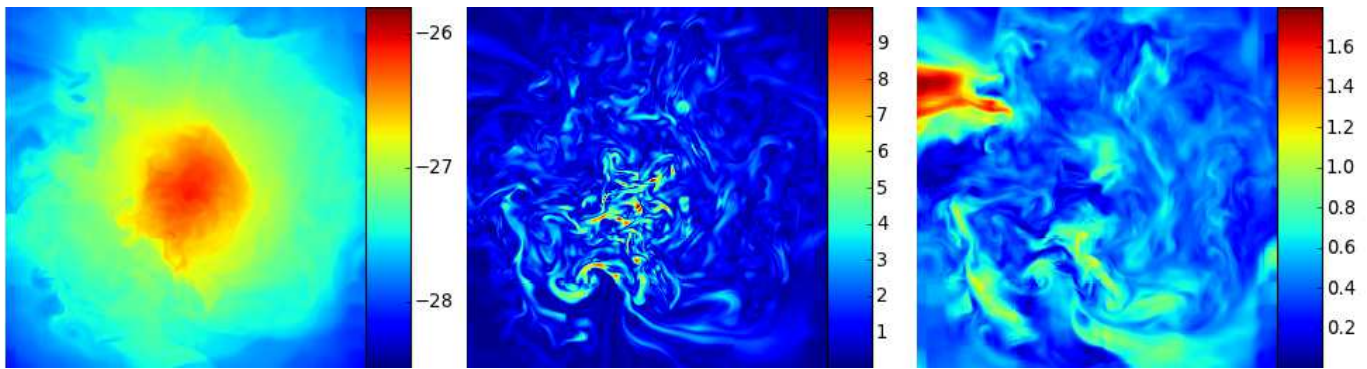


FIG. 1.— A slice through the center of a simulated cluster data (3 Mpc across) – log density  $\log_{10}(\rho g^{-1} \text{cm}^3)$  (left), RMS magnetic field,  $\mu\text{G}$  (middle) and RMS velocity,  $10^8 \text{ cm/s}$  (right). Typical sound speed  $c_s \sim 10^8 \text{ cm/s}$ , typical Alfvén speed  $v_A \sim 10^7 \text{ cm/s}$ .

tion, including mergers from infalling objects and accretion of gas, are becoming more and more popular recently (see, e.g. Nagai et al. 2007; Borgani & Kravtsov 2009; Dolag & Stasyszyn 2009; Xu et al. 2010; Donnert et al. 2011, , etc). These simulations produce magnetic fields which are roughly consistent with the observed rotation measures (see, e.g. Xu et al. 2012) . Thus, one can hope to elicit the properties of small-scale ICM turbulence and predict the effects of second-order acceleration. Obviously, it is impossible to reach scales of CR gyroradius in a cosmological cluster simulation, so the subgrid model of turbulence has to be adopted.

In §2 we discuss the origin of cluster magnetic field, in §3 we present the setup of our cosmological simulations, in §4 we describe compressible turbulence in the ICM, in §5 we propose a novel technique to decompose ICM turbulent perturbations into MHD modes, in §6 we discuss diffusive CR acceleration by the fast mode and in §7 we summarize our findings.

## 2. SMALL-SCALE DYNAMO

The strength of primordial magnetic fields is still unknown<sup>1</sup> with the upper bound around  $10^{-9} \text{ G}$  (Paoletti & Finelli 2011; Schleicher & Miniati 2011). Assuming that clusters formed as a result of a gravitational collapse of an unmagnetized gas, a proper mechanism of generating observed magnetic fields in the ICM has to be pointed out. Taking into account that the cluster volume is several cubic megaparsecs, the magnetic field provided directly by galactic winds and AGN lobes are grossly insufficient and the observed field has to be amplified in situ by cluster turbulence. Typically, the outer scales of cluster magnetic fields estimated from observations (Carilli & Taylor 2002) are much smaller than turbulence outer scales, which is why cluster dynamo is normally the small-scale dynamo. Also, generating large-scale fields, i.e. larger than an outer scale of turbulence, such as those observed in spiral galaxies, requires many (typically hundreds) dynamical timescales of turbulence

<sup>1</sup> A lower bounds based on the argument that FERMI did not observe GeV photons from inverse Compton scattering of the CMB by the electron-positron pair cascade has been suggested by Neronov & Vovk (2010); Tavecchio et al. (2010), but has been debated recently by the beam instability argument by Broderick et al. (2012); Schlickeiser et al. (2012). However, another lower bound of  $\delta B = 10^{-19} \text{ G}(n/10^{-3} \text{ cm}^{-3})(T/10^7 \text{ K})^{-3/4}$  based on basic plasma processes has been proposed recently by Schlickeiser (2012).

on the driving scale, which is impossible in the ICM, where dynamical timescale is comparable with the age of the Universe.

Although Coulomb mean-free path (mfp) of a thermal particle in the ICM is very large, 10-100kpc, it is believed that the actual mean free path is much smaller due to magnetic fields and turbulence. Indeed, the Larmor radius of a thermal particle in a  $1 \mu\text{G}$  field is  $10^{-9} \text{ pc}$  and even if we assume that particles stream freely along tangled magnetic field, the mfp will be greatly reduced. Further reduction of mfp is very likely due to scattering by collective effects (Schekochihin & Cowley 2006; Lazarian & Beresnyak 2006; Schekochihin et al. 2008), with estimates of the mfp between  $10^{-3}$  and  $10^{-6} \text{ pc}$ . The cluster environment, therefore, is unlikely to be kinetic-viscous, as was commonly suggested before based on Coulomb mfp, but rather a high-Reynolds number ( $Re$ ) turbulent environment, with self-similar scalings for velocity covering many orders of magnitude. While the kinematic dynamo, which ignored the backreaction of the magnetic field, has been studied extensively, due to the relative simplicity of the approach, the nonlinear small-scale dynamo received less attention. In high- $Re$  environments kinematic dynamo saturates very quickly, giving way to the nonlinear regime.

Nonlinear small-scale dynamo has been studied extensively only recently. In particular, numerical simulations have established that the saturated state of such dynamo is relatively unaffected by  $Re$ , as long as  $Re$  is large (Haugen et al. 2004). It was suggested that the small-scale dynamo in large  $Re$  flows could be universal (Schlüter & Biermann 1950; Schekochihin & Cowley 2007) and this was supported by further numerical and analytical studies (Cho et al. 2009; Beresnyak et al. 2009), in particular the universality of the homogeneous small-scale dynamo based on turbulence locality has been argued in Beresnyak (2012). Although real clusters are not homogeneous, small-scale turbulence could be considered approximately homogeneous on scales which are much smaller than cluster size. In this case the growth rate of magnetic energy is proportional to the local turbulence dissipation rate with a coefficient of around 0.05 (Beresnyak 2012).

Full self-consistent MHD simulations of galaxy cluster formation, such as those presented here, are, in principle, able to model the small-scale dynamo in clusters. However, due to the much lower effective  $Re$ , such sim-

ulations tend to prolong the initial exponential growth period. A balance have to be found between realistic magnetic injection mechanism, such as AGN activity in Xu et al. (2010) or galaxy winds in Donnert et al. (2009) and the aforementioned artificial delay of growth. Since the magnetic fields obtained in simulations by Xu et al. (2012) that we use in this paper are consistent with observations, we will assume that they adequately reproduce the small-scale dynamo action in clusters.

### 3. CLUSTER SIMULATIONS

The galaxy cluster studied in this paper is the simulation A in Xu et al. (2010). This simulation is performed using the cosmological MHD code with adaptive mesh refinement (AMR) ENZO+MHD (Collins et al. 2010). The simulation here uses an adiabatic equation of state, with the ratio of specific heat being 5/3, and does not include heating and cooling physics or chemical reactions, which are not important in this research.

The initial conditions of the simulation are generated at redshift  $z = 30$  from an Eisenstein & Hu (1999) power spectrum of density fluctuation in a  $\Lambda$ CDM universe with parameters  $h = 0.73$ ,  $\Omega_m = 0.27$ ,  $\Omega_b = 0.044$ ,  $\Omega_\Lambda = 0.73$ , and  $\sigma_8 = 0.77$ . These parameters are close to the values from WMAP3 observations (Spergel et al. 2007). The simulation volume is  $(256 h^{-1} \text{Mpc})^3$ , and it uses a  $128^3$  root grid and 2 level nested static grids in the Lagrangian region where the cluster forms. This gives an effective root grid resolution of  $512^3$  cells ( $\sim 0.69$  Mpc) and dark matter particle mass resolution of  $1.07 \times 10^{10} M_\odot$ . During the course of the simulation, 8 levels of refinements are allowed beyond the root grid, for a maximum spatial resolution of  $7.8125 h^{-1}$  kpc. The AMR is applied only in a region of  $(\sim 43 \text{Mpc})^3$  where the galaxy cluster forms near the center of the simulation domain. The AMR criteria in this simulation are follows. During the cluster formation but before the magnetic fields are injected, in addition to the density refinement, the refinement is controlled by baryon and dark matter density. After magnetic field injections, all the regions where magnetic field strengths are higher than  $5 \times 10^{-8}$  G are refined to the highest level.

The magnetic field initialization is using the same method in Xu et al. (2008, 2009) as the original model proposed by Li et al. (2006) assuming that the magnetic fields are from the outburst of an AGN. We have the magnetic fields injected at redshift  $z = 3$  in the most massive halo of  $1.5 \times 10^{13} M_\odot$ . We assume that the magnetic fields are from  $\sim 10^9 M_\odot$  supermassive black hole with about 1% of outburst energy in magnetic form. There is  $\sim 1.9 \times 10^{60}$  erg magnetic energy put into the ICM. Previous study (Xu et al. 2010) has shown that the injection redshifts and magnetic energy are not important to the distributions of the ICM magnetic fields at low redshifts.

The simulated cluster is a massive cluster with its basic properties at redshift  $z = 0$  as follows:  $R_{\text{virial}} = 2.16$  Mpc,  $M_{\text{virial}}(\text{total}) = 1.25 \times 10^{15} M_\odot$ ,  $M_{\text{virial}}(\text{gas}) = 1.86 \times 10^{14} M_\odot$ , and  $T_{\text{virial}} = 7.65$  keV. This cluster is already relaxed at the current epoch in the sense of X-ray and density distribution, but the turbulence is still excited by recent minor mergers. The final total magnetic energy is  $1.43 \times 10^{61}$  erg. The details about the cluster formation and magnetic field evolution are presented in Xu et al. (2010). We visualized three quantities from a

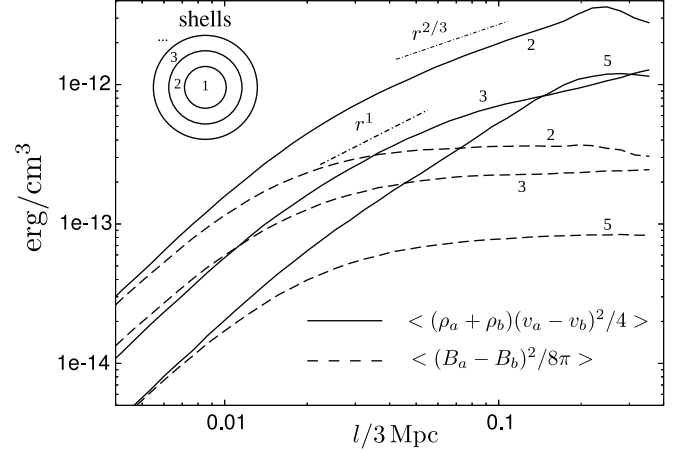


FIG. 2.— Second order structure functions, characterizing kinetic (solid) and magnetic (dashed) energy density in clusters. Here  $\rho_a, \rho_b, v_a, v_b, B_a, B_b$  are the quantities taken at points a and b, separated by distance  $l$ . The middle point between a and b lies within a shell, whose number is indicated above the data. The outer radius of  $n$ th shell is  $n \cdot 300$  kpc. We use structure function method to calculate these quantities in shells around cluster center, since all quantities depend strongly on the distance to the center.

simulation slice in Fig. 1.

### 4. COMPRESSIBLE MHD TURBULENCE IN THE ICM

These simulations reveal that the dominant mechanism of the excitation of the cluster-wide turbulence in the galaxy cluster medium is cluster mergers (see, e.g., Vazza et al. 2011; Xu et al. 2010; Donnert et al. 2011). Since the typical infall velocity and the typical thermal sound speed are related to virial velocity, they are of the same order, so the infall is typically trans-sonic, generating a sizable amount of compressive perturbations and, possibly, weak shocks. Another mechanism could be due to bringing hot plasma inside cooler core environment, where the hot gas will become buoyant and produce convective turbulence and mixing in the center.

Speaking of turbulence in the ICM, a simplified approach is often taken when a turbulence is characterized by the local characteristic gas velocity (Iapichino & Niemeyer 2008; Vazza et al. 2009; Donnert et al. 2011). This will not be sufficient, however, if one wants to address the issue of second order acceleration. Indeed, the quasi-incompressible component of MHD turbulence, consisting of slow and Alfvén modes tend to become progressively more anisotropic on smaller scales (Goldreich & Sridhar 1995) and, in a test particle limit, effectively decouples from cosmic rays (CRs) (Chandran 2000; Yan & Lazarian 2002, 2004). Therefore, we want to know the fraction of the fast mode, produced by cluster turbulence, which up till now has not been reliably estimated. In this paper we will estimate the ratio of turbulent energy in each mode from simulation data and our subgrid model of turbulence will assume independent energy cascades for each mode as in Cho et al. (2003)<sup>2</sup>.

<sup>2</sup> The question of mode coupling is outside the scope of this paper, however a few comments could be made. In particular, the absence of energy exchange between slow and Alfvénic mode on small scales in a weakly compressible case can be argued on rigorous basis, even if the interaction between modes is strong, i.e.

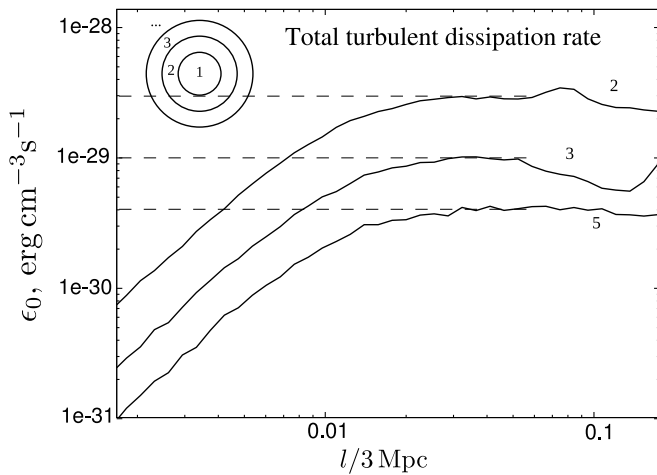


FIG. 3.— Turbulent dissipation rate in clusters, calculated with third order structure functions in three shells. Combined with the previous data, this allows us to estimate dynamic lifetime of turbulence in cluster, which is  $3 \cdot 10^9$  years in shells 2-3 and  $8 \cdot 10^9$  years in shell 5.

Estimating mode ratios is a fairly challenging task, because the magnetic field in clusters is tangled and has no global mean field component, so global Fourier transforms of turbulent fields over the whole cluster could not be decomposed into modes. Also, doing global Fourier transforms in a datacube containing a whole cluster is rather meaningless, since all quantities strongly depend on the distance to the cluster center. So, the power spectra obtained from such transforms will be severely contaminated by large-scale gradients. In this paper we propose and use a local decomposition method based on structure functions (SFs). This is the first time such a method is used with the ICM MHD turbulence. This method also allows us to reduce the error associated with the fact that the cluster is not uniform and any measurement will include large-scale gradients associated with the cluster shape. In particular all global velocity measurements are contaminated by global accretion flow. The attempts to subtract this flow based on careful modelling of the averaged flow has not been either simple or reliable.

The second order structure function is directly related to the power spectrum in the homogeneous case, e.g. the second order structure function scaling  $r^m$  corresponds to the power spectrum scaling of  $k^{-m-1}$  ( $0 < m < 2$ ). In the inhomogeneous case, the structure function will act as a good proxy for determining the local power spectrum of turbulence. The main idea of our method is to use volume averaged structure function in shells centered on the cluster center. We are able to do so because the structure function is a local measurement. We used five shells with radii increasing linearly by 300 kpc for each shell. Fig. 2 shows second-order structure functions corresponding to the kinetic and magnetic energy densities in the cluster. Note that the power spectra in different shells differ by orders of magnitude. This further reiterates the need to use local measurement, rather than the global Fourier transform.

Fig. 3 shows turbulence energy flux, calculated locally

perturbative theory is impossible, see, e.g., Goldreich & Sridhar (1995); Beresnyak (2011).

by a well-known method of third-order structure functions (see, e.g., Politano & Pouquet 1998). We can apply this method because cluster turbulence is only weakly compressive. Our energy fluxes correspond to the turbulence decay times of several billion years. This is a reasonable number for a quiet cluster. Note that if we assume that the cluster center is as hot as in our adiabatic simulations, the bremsstrahlung cooling in the center,  $\sim 10^{-27} \text{erg cm}^{-3} \text{s}^{-1}$  will be a factor of  $\sim 30$  larger than the turbulent heating rate in shell one. Turbulent heating is unable to compete with cooling. This is expected, however, since it is turbulent mixing which is primarily responsible for heating the center. Indeed, if  $\tau$  is the turbulence mixing time, then turbulent dissipation is  $\rho v^2 / \tau$ , but the heating from mixing can be estimated as  $nT(l/l_T)/\tau$ , where  $l_T$  is a temperature gradient scale and  $l$  is the turbulence outer scale. We expect turbulence to come from mergers and have outer scales as large as the cluster size, i.e.  $l/l_T \sim 1$ . On the other hand,  $nT \gg \rho v^2$  as clusters are subsonic. If  $M_s$  is an RMS sonic Mach number of cluster turbulence, the turbulent mixing provides approximately  $1/M_s^2$  times more heating of the cluster core than direct turbulent dissipation.

## 5. MODE DECOMPOSITION IN MHD TURBULENCE

MHD mode decomposition in turbulence, based on Fourier transforms has been used before by Cho & Lazarian (2002); Cho et al. (2003); Cho & Lazarian (2003). In these papers the global Fourier transform provided a global wavevector  $\mathbf{k}$  for each Fourier mode, therefore necessitating the use of a global mean field. Indeed the global mean field was relatively strong in all aforementioned simulations, resulting in trans-Alfvenic turbulence. This approach works in the interstellar medium (ISM) of spiral galaxies where the turbulent component of the field is comparable with the mean-field component (see, e.g., Schlickeiser 2002). In galaxy clusters such an approach is impossible due to the lack of a global mean field. The wavelet technique has been proposed to deal with this difficulty in Kowal & Lazarian (2010). The wavelet technique is computationally expensive, however, and requires datacubes with reduced resolution. Also, it has been only applied to homogeneous turbulence. The case of cluster turbulence is especially difficult, since not only cluster turbulence has no mean magnetic field, but also it is strongly inhomogeneous with density changing several orders of magnitude from the center to the outskirts of the cluster. In this paper we use a hybrid approach based on both Fourier transforms and structure functions. As was described in previous sections, since structure functions are local measurements we can calculate them in shells around the cluster center, therefore mitigating effects associated with large scale gradient along the radius.

As cluster turbulence exists in a very hot gas,  $\sim 10^7 \text{K}$ , the gas pressure is typically higher than dynamic pressure in most of the volume, resulting in subsonic turbulence with  $M_s \ll 1$ . Out of three MHD modes, Alfvén mode is precisely incompressible, due to  $\mathbf{k}$  being perpendicular to both  $\mathbf{B}$  and  $\delta \mathbf{v}$ . Slow and fast modes are both compressible, but the slow mode is almost incompressible in subsonic, high- $\beta$  case. We can, therefore, split modes in two groups, one of them is almost incom-

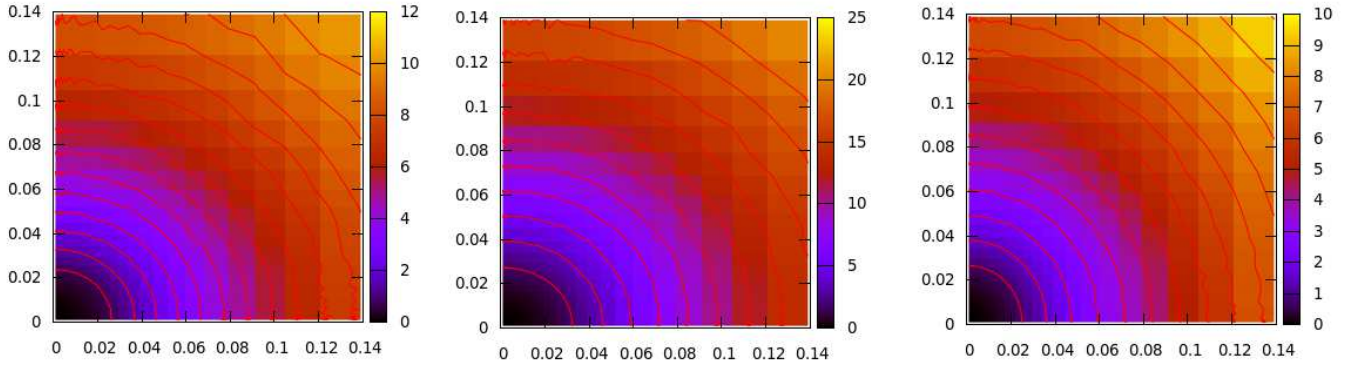


FIG. 4.— Second order structure functions of Alfvénic (left), slow (middle) and fast (right) mode, calculated with respect to the local magnetic field, x axis is along magnetic field, while y axis is perpendicular to the field. Unit of structure function is  $10^{14} \text{cm}^2/\text{s}^2$ , unit of length on x and y axis is the box size, which is 3 Mpc. Alfvénic and slow mode eddies show small anisotropy along  $\mathbf{B}$ , the anisotropy is small due to very short range of MHD scales, as the MHD scale is close to dissipation scale. Fast mode shows slight inverse anisotropy.

pressible Alfvén and slow mode and the other is fully compressible fast mode. In high- $\beta$  case fast mode speed is close to sonic speed  $c_s$  and the dispersion relation is almost isotropic.

Figure 4 shows the structure of the modes using contours of the second-order structure function plotted with x axis corresponding to the direction along magnetic field and y axis to perpendicular direction. The contours approximate the averaged shape of “turbulent eddies”. We see that Alfvénic and slow modes show fairly small anisotropy along  $\mathbf{B}$ , which is due to the fact that we have very short inertial range for MHD turbulence (below MHD scale). Fast mode shows slight inverse anisotropy. It was often assumed earlier that the fast mode turbulence is intrinsically isotropic. It is not true, however, since the weak cascade of the fast mode consists of independent cascades along rays in  $\mathbf{k}$ -space, so it will preserve any anisotropy which is originally present. The scattering by other modes is expected to be small on small scales and the cascade rate for each individual ray is a strong function of the angle between  $\mathbf{k}$  and  $\mathbf{B}$ .

Figure 5 shows the second order structure function for velocity component corresponding to the fast mode. It turns out that the fraction  $e_f$  of kinetic energy residing in the fast mode is considerable. We studied this fraction by taking the ratio of the fast mode component second order structure function to the total velocity second order structure function and found that this ratio was around  $e_f \sim 0.25$  for all shells. This contrasts with the analytical estimate used in Brunetti & Lazarian (2011a), which gives the small fraction  $\sim M_s^2/M_A$  for subsonic clusters. The analytical estimate in the aforementioned paper was based on periodic box simulations with solenoidal driving that typically produces very small amount of fast mode (Cho & Lazarian 2003). In clusters, however, most of the turbulent energy is supplied due to mergers which have compressible and trans-sonic velocity fields, since the infall velocity is of the order of sonic speed which is virial on the outskirts of the cluster. This explains the difference between the estimate in Brunetti & Lazarian (2011a) and our calculation of  $e_f$  from simulated cluster.

Since the typical Mach numbers in the cluster center are modest  $M_s \sim 0.3$ , we will assume that the fast mode supplies a small fraction of the total dissipation rate,

$\epsilon \sim \epsilon_0 e_f^2 M_s \sim 0.02 \epsilon_0$ . On the outskirts of the cluster this fraction is higher, due to  $M_s \sim 1$ , but the estimates of fast mode amplitudes on the outskirts are only tentative, due to limited numerical resolution.

For the fast mode scaling we will use the so-called weak turbulence model, which was suggested in (Cho et al. 2003). The power spectrum of fast mode fluctuations, assuming their isotropy, which is roughly consistent with Fig. 5, can be expressed phenomenologically as

$$E_F(k) = C_{KF} \epsilon^{1/2} c_s^{1/2} k^{-3/2}, \quad (1)$$

where  $C_{KF}$  is the Kolmogorov constant for weak turbulence. Note that the constant in this form is implicitly averaged over angle, since the weak cascade happens independently along each ray in  $\mathbf{k}$ -space. For the purpose of this paper, however, we will only need the assumption that the spectrum is approximately isotropic.

## 6. IMPLICATIONS FOR CR ACCELERATION

In this section we will briefly outline the consequences of the significant amount of fast mode found in our cluster simulations. We will use simplified expressions for second-order acceleration, dropping out numerical factors of order unity. More detailed calculation of acceleration, although based on the above mentioned analytical estimate of the amplitude of the fast mode, can be found in Brunetti & Lazarian (2011a,b). We also expect additional factors from the fact that the fast mode, excited by cluster turbulence, is not exactly isotropic.

Second-order acceleration by turbulence has been suggested as a process that provides additional energy to secondary electrons and allows them to produce an observable amount of radio emission. Energetically, it is hard to support large amounts of fast electrons just by protons alone, and even if it was possible such sources will have much brighter cores than observed (see, e.g., Donnert et al. 2011). The attractiveness of second-order acceleration models is that it will produce relatively featureless radio halos, similar to the observed halos, since turbulence is volume-filling. If, on the other hand, most of the acceleration happens in the accretion shocks, they will produce a different observed morphology, due to relatively short lifetimes of synchrotron electrons. Indeed, so-called radio relics, which morphologically re-

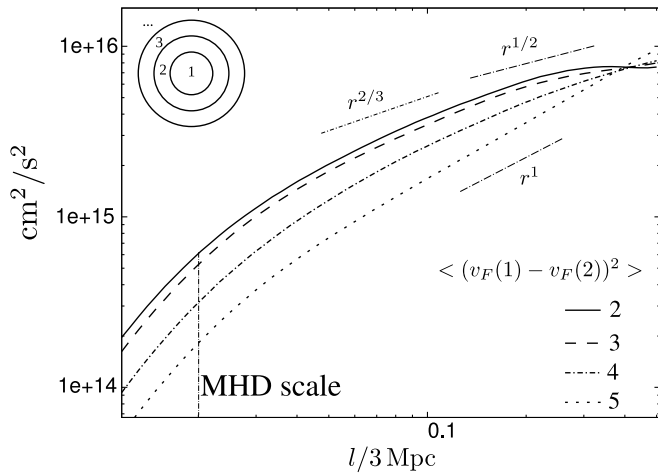


FIG. 5.— Second order structure function of the fast mode component of velocity, where the vector between points a and b was chosen to be perpendicular to the cluster center to exclude contribution from the accretion flow. Note that due to the poor resolution at the outskirts of the cluster (shells 4-5) the scaling is very steep, i.e. turbulent scaling is not observed. This allows us to estimate the amplitude of the fast mode perturbations only in the inside shells (1-3).

semble large-scale shocks, has been observed in some clusters (Ensslin et al. 1998). Although we can not exclude shock acceleration in ordinary radio haloes, due to either face-on shock geometry or multiple small-scale shocks (see, e.g. van Weeren et al. 2010), in this paper we will investigate primarily the volume-filling second-order acceleration, which is the most natural explanation of megaparsec-scale radio haloes.

Second-order acceleration is a diffusion of particles in the momentum space due to collision with magnetic irregularities. The original mechanism, proposed by Fermi (1949), assumed collisions with large-scale clouds, while turbulence models assume resonant interaction with MHD modes. The flux of particles through momentum space due to momentum diffusion is defined as  $F = -4\pi p^2 D_{pp} \partial f / \partial p$ , where we assumed isotropy and have used the momentum diffusion coefficient  $D_{pp}$  already integrated over the pitch angle. This  $D_{pp}$  is equivalent to  $A_2$  from Schlickeiser (2002). This term provides acceleration, as long as  $\partial f / \partial p < 0$ , which is normally satisfied. The estimate of momentum diffusion due to the interaction with fast mode as  $D_{pp} = p^2 v_A^2 L_M^{-1/2} c^{-1} (pc/eB)^{-1/2}$ , where  $L_M$  is the MHD scale (see, e.g., Schlickeiser 2002; Yan & Lazarian 2004). We dropped out all factors of order unity, although they can also be absorbed in the parameter  $L_M$ . If we assume that this process is dominant over space diffusion and losses, then the stationary solution will correspond to  $F = \text{const}$  which suggests that  $f \sim p^{-5/2}$ , corresponding to the energy distribution  $E_p = 4\pi p^2 f \sim p^{-1/2}$ , a very flat spectral index, compared with observed spectral indices which are between  $-2$  and  $-4$ . This flatness is an inevitable feature of second-order acceleration, because particles try to diffuse to higher  $p$  where there is a larger phase volume. If escape due to diffusion is taken into account, the result is virtually unchanged as long as particles are well-trapped, i.e. acceleration timescales are smaller than the diffusive escape timescales. If, on the other hand, escape

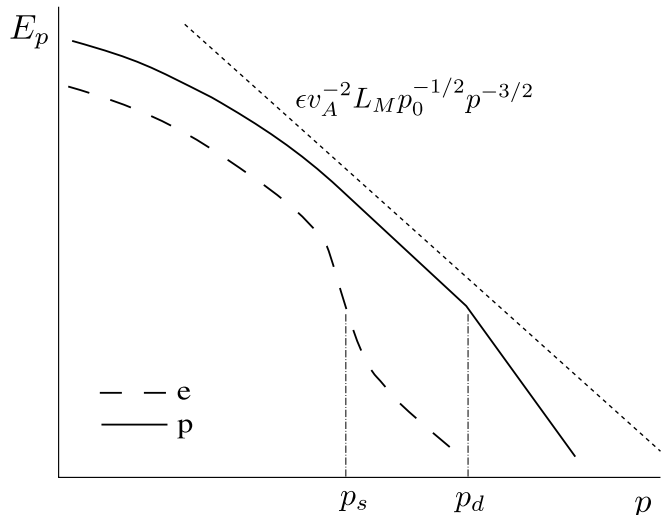


FIG. 6.— Spectra of electrons and protons, reaccelerated by fast mode turbulence in the galaxy cluster. The proton spectrum is limited from above by absolute energetic constraint of Eq. (2). The  $e/p$  ratio initially corresponds to the injection  $e/p$  ratio till the electron synchrotron suppression at  $p_s$ . This ratio will increase later due to secondary  $e^\pm$  production. For higher energies  $e/p$  ratio is smaller, as electron spectrum is in equilibrium between production directly from protons and synchrotron losses.

is more efficient, the second-order acceleration will only slightly modify the injected particle distribution (see, e.g. Schlickeiser 2002). The radio emission spectra of halos are rather steep, which suggests steep particle distributions and it would seem that second-order acceleration will either be inefficient or produce particle distributions which are clearly incompatible with the observed ones. However, in practice a variety of other effects have to taken into account. Synchrotron cooling is one of these effects, it could be expressed as  $F = -4\pi p^2 \dot{p} f$ , where  $\dot{p} \sim p^2$ . This will result in a cutoff of accelerated distribution, in a form  $E_p \sim p^{-1/2} \exp(-(p/p_s)^{3/2})$ , where  $p_s$  is a cutoff momentum. This cutoff will result in a steeper emitted radio spectra and these spectra can be mistakenly identified as produced by steep  $E_p$  distributions.

We argue, however, that another process of fundamental importance is operating in second-order acceleration, which is the back-reaction of particles to turbulence. Indeed, there is an energetic constrain that requires that CRs should not extract more energy than that is available in the turbulent cascade. If this condition is ignored and turbulent spectra are postulated to be power-law, an excessive amount of particle heating will be obtained. The turbulent cascade can produce classic self-similar solutions, such as  $\delta B^2 \sim k^{-1/2}$  for the fast mode, only when the back-reaction to turbulence is ignored and the energy flux is due to fluid nonlinearity alone and is constant through all scales. In practice, this condition will be quickly broken by the feedback of CRs.

An absolute upper limit on second-order acceleration could be obtained by assuming that the energy extracted on each scale should not exceed large scale turbulent dissipation rate  $\epsilon$ . As the flux of energy in accelerated particles can be expressed as  $F_E = pcF = -4\pi cp^3 D_{pp} \partial f / \partial p$ , this upper limit will result in an upper limit on  $E_p < p^{-1.5}$ , which is steeper than constant particle flux solution, suggesting that unless second-order acceleration is

limited by losses or escape, it will eventually be limited at high energies by back-reaction to turbulence. Assuming that protons take most of the turbulent energy the  $E_p$  will be limited from above by

$$E_p < \epsilon v_A^{-2} L_M p_0^{-1/2} p^{-3/2}, \quad (2)$$

where  $L_M$  is the MHD scale of fast mode turbulence,  $p_0 \approx 12eBL_M/c$ . The transition to steeper spectra possibly generated by other mechanisms happens at a momentum  $p_d$ , which will be determined by the total turbulent energetic history of the cluster and is approximately related to the temperature on the outskirts of the cluster. Assuming turbulence pumping 30% of the time with the dissipation rate of  $\epsilon$  during the age of the Universe  $t_A$ , we obtain the expression  $p_d = p_0(0.15t_A v_A^2/cL_M)^2$ . Numerically it could be estimated assuming  $v_A \sim 10^7$  cm/s and  $L_M \sim 60$  kpc as  $p_d \sim 2 \cdot 10^{-6} p_0 \sim 2 \cdot 10^{15}$  eV/c, so the maximum proton gyroradius is still much smaller than MHD scale  $L_M$ . This is due to second-order acceleration being a rather inefficient acceleration mechanism.

As for the electrons, their cutoff energy  $p_s$  will be determined by the balance between synchrotron cooling and momentum diffusion as  $p_s = m_e c(16\pi^2 e B m_e c^2 / \sigma_T^2 L_M B_*^4)^{1/3} (v_A/c)^{4/3}$ , where  $B_* = (B^2 + B_{IC}^2)^{1/2}$  includes equivalent  $B_{IC} \sim 3(1+z)^2 \mu\text{G}$  to account for inverse Compton losses on CMB and synchrotron losses. Using parameters from above,  $p_s \sim 4 \cdot 10^4 m_e c$ . The sketch of the electron and proton spectra are presented in Fig. 6. The sharp cutoff in electron spectra, associated with transition from the spectrum of accelerated electrons to the spectrum of secondary electrons could explain the relatively steep spectra of radio emission from radio halos.

## 7. SUMMARY

The nonthermal radiation from hot conductive intra-cluster medium (ICM) is explained by the presence of accelerated particles. It is plausible that the cause of acceleration, in the case of radio halos, is not large-scale accretion shocks, but rather volumetric turbulence that is produced by constant mergers and buoyancy of the cluster medium. This turbulence is currently being investigated by cosmological MHD simulations as being a source of both magnetic fields and accelerated particles. The key to in-situ acceleration of electrons and protons is the MHD fast mode which effectively scatter particles and diffusively accelerate them. We propose a novel method to extract fast mode from MHD simulation and estimate the efficiency of acceleration and scattering. An important limit, imposed by the energy flux constraint of the fast mode turbulence leads to a spectrum which is steeper than one would naively assume from diffusive acceleration. Moreover, this spectrum has an exponential cutoff at relatively low energies for electrons which could naturally explain very soft radio spectra typically observed for diffuse radio halos. A more detailed calculation of the particle distribution in space and simulated radio maps will be presented in a future publication.

## 8. ACKNOWLEDGMENTS

AB is grateful to Gianfranco Brunetti and Julius Donert for illuminating discussions. AB was supported by Humboldt Fellowship at the Ruhr-Universität Bochum and Los Alamos Director's Fellowship. HX and HL are supported by the LDRD and IGPP programs at LANL and by DOE/Office of Fusion Energy Science through CMSO. RS acknowledges partial support by the Deutsche Forschungsgemeinschaft (grant Schl 201/25-1).

## REFERENCES

- Ackermann, M., Ajello, M., Allafort, A., Baldini, L., Ballet, J., et al. 2010, *The Astrophysical Journal Letters*, 717, L71
- Beresnyak, A. 2011, *Phys. Rev. Lett.*, 106, 075001
- , 2012, *Phys. Rev. Lett.*, 108, 035002
- Beresnyak, A., Jones, T. W., & Lazarian, A. 2009, *ApJ*, 707, 1541
- Bonafede, A., Feretti, L., Murgia, M., Govoni, F., Giovannini, G., Dallacasa, D., Dolag, K., & Taylor, G. B. 2010, *A&A*, 513, A30
- Borgani, S., & Kravtsov, A. 2009, *ArXiv e-prints*
- Broderick, A. E., Chang, P., & Pfrommer, C. 2012, *ApJ*, 752, 22
- Brunetti, G., & Lazarian, A. 2011a, *MNRAS*, 410, 127
- , 2011b, *MNRAS*, 412, 817
- Brunetti, G., Giacintucci, S., Cassano, R., Lane, W., Dallacasa, D., et al. 2008, *Nature*, 455, 944
- Carilli, C. L., & Taylor, G. B. 2002, *ARA&A*, 40, 319
- Cassano, R., Brunetti, G., Setti, G., Govoni, F., & Dolag, K. 2007, *MNRAS*, 378, 1565
- Chandran, B. D. G. 2000, *Physical Review Letters*, 85, 4656
- Cho, J., & Lazarian, A. 2002, *Phys. Rev. Lett.*, 88, 245001
- , 2003, *MNRAS*, 345, 325
- Cho, J., Lazarian, A., & Vishniac, E. T. 2003, in *Lecture Notes in Physics*, Berlin Springer Verlag, Vol. 614, Turbulence and Magnetic Fields in Astrophysics, ed. E. Falgarone & T. Passot, 56–98
- Cho, J., Vishniac, E. T., Beresnyak, A., Lazarian, A., & Ryu, D. 2009, *ApJ*, 693, 1449
- Collins, D. C., Xu, H., Norman, M. L., Li, H., & Li, S. 2010, *ApJS*, 186, 308
- Dennison, B. 1980, *ApJ*, 239, L93
- Dolag, K., & Staszczyn, F. 2009, *MNRAS*, 398, 1678
- Donert, J., Dolag, K., Cassano, R., & Brunetti, G. 2011, *Mem. Soc. Astron. Italiana*, 82, 623
- Donert, J., Dolag, K., Lesch, H., & Müller, E. 2009, *MNRAS*, 392, 1008
- Eilek, J. A., & Owen, F. N. 2002, *ApJ*, 567, 202
- Eisenstein, D. J., & Hu, W. 1999, *ApJ*, 511, 5
- Ensslin, T. A., Biermann, P. L., Klein, U., & Kohle, S. 1998, *A&A*, 332, 395
- Feretti, L., Giovannini, G., Govoni, F., & Murgia, M. 2012, *A&A Rev.*, 20, 54
- Fermi, E. 1949, *Physical Review*, 75, 1169
- Ferrari, C., Govoni, F., Schindler, S., Bykov, A. M., & Rephaeli, Y. 2008, *Space Sci. Rev.*, 134, 93
- Giovannini, G., Bonafede, A., Feretti, L., Govoni, F., Murgia, M., Ferrari, F., & Monti, G. 2009, *A&A*, 507, 1257
- Giovannini, G., Tordi, M., & Feretti, L. 1999, *New Astronomy*, 4, 141
- Goldreich, P., & Sridhar, S. 1995, *ApJ*, 438, 763
- Govoni, F., Murgia, M., Feretti, L., Giovannini, G., Dolag, K., & Taylor, G. B. 2006, *A&A*, 460, 425
- Govoni, F., Dolag, K., Murgia, M., Feretti, L., Schindler, S., et al. 2010, *A&A*, 522, A105
- Haugen, N. E., Brandenburg, A., & Dobler, W. 2004, *Phys. Rev. E*, 70, 016308
- Hoefl, M., Brüggem, M., Yepes, G., Gottlöber, S., & Schwobe, A. 2008, *MNRAS*, 391, 1511
- Iapichino, L., & Niemeyer, J. C. 2008, *MNRAS*, 388, 1089
- Jaffe, W. J. 1977, *ApJ*, 216, 212
- Kowal, G., & Lazarian, A. 2010, *ApJ*, 720, 742
- Lazarian, A., & Beresnyak, A. 2006, *MNRAS*, 373, 1195
- Li, H., Lapenta, G., Finn, J. M., Li, S., & Colgate, S. A. 2006, *ApJ*, 643, 92
- McNamara, B. R., & Nulsen, P. E. J. 2007, *ARA&A*, 45, 117

- Motl, P. M., Hallman, E. J., Burns, J. O., & Norman, M. L. 2005, *ApJ*, 623, L63
- Nagai, D., Vikhlinin, A., & Kravtsov, A. V. 2007, *ApJ*, 655, 98
- Neronov, A., & Vovk, I. 2010, *Science*, 328, 73
- Paoletti, D., & Finelli, F. 2011, *Phys. Rev. D*, 83, 123533
- Politano, H., & Pouquet, A. 1998, *Phys. Rev. E*, 57, R21
- Reimer, A., Reimer, O., Schlickeiser, R., & Iyudin, A. 2004, *A&A*, 424, 773
- Rephaeli, Y. 1977, *The Astrophysical Journal*, 212, 608
- Schekochihin, A. A., & Cowley, S. C. 2006, *Physics of Plasmas*, 13, 056501
- . 2007, *Turbulence and Magnetic Fields in Astrophysical Plasmas* (Springer), 85–+
- Schekochihin, A. A., Cowley, S. C., Kulsrud, R. M., Rosin, M. S., & Heinemann, T. 2008, *Physical Review Letters*, 100, 081301
- Schleicher, D. R. G., & Miniati, F. 2011, *MNRAS*, 418, L143
- Schlickeiser, R. 2002, *Cosmic Ray Astrophysics* (Springer)
- . 2012, *Physical Review Letters*, 109, 261101
- Schlickeiser, R., Ibscher, D., & Supsar, M. 2012, *ApJ*, 758, 102
- Schlickeiser, R., Sievers, A., & Thiemann, H. 1987, *A&A*, 182, 21
- Schlüter, A., & Biermann, I. 1950, *Zeitschrift Naturforschung Teil A*, 5, 237
- Skillman, S. W., Hallman, E. J., O’Shea, B. W., Burns, J. O., Smith, B. D., & Turk, M. J. 2011, *ApJ*, 735, 96
- Spergel, D. N., Bean, R., Doré, O., Nolta, M. R., Bennett, C. L., et al. 2007, *ApJS*, 170, 377
- Tavecchio, F., Ghisellini, G., Foschini, L., Bonnoli, G., Ghirlanda, G., & Coppi, P. 2010, *MNRAS*, 406, L70
- van Weeren, R. J., Röttgering, H. J. A., Brügger, M., & Hoeft, M. 2010, *Science*, 330, 347
- van Weeren, R. J., Röttgering, H. J. A., Rafferty, D. A., Pizzo, R., Bonafede, A., et al. 2012, *A&A*, 543, A43
- Vazza, F., Brunetti, G., Gheller, C., Brunino, R., & Brügger, M. 2011, *A&A*, 529, A17
- Vazza, F., Brunetti, G., Kritsuk, A., Wagner, R., Gheller, C., & Norman, M. 2009, *A&A*, 504, 33
- Xu, H., Li, H., Collins, D., Li, S., & Norman, M. L. 2008, *ApJ*, 681, L61
- Xu, H., Li, H., Collins, D. C., Li, S., & Norman, M. L. 2009, *ApJ*, 698, L14
- . 2010, *ApJ*, 725, 2152
- Xu, H., Govoni, F., Murgia, M., Li, H., Collins, D. C., et al. 2012, *ApJ*, 759, 40
- Yan, H., & Lazarian, A. 2002, *Phys. Rev. Lett.*, 89, B1102
- . 2004, *ApJ*, 614, 757